A Modified Carrier-Based DPWM With Reduced Switching Loss and Current Distortion for Vienna Rectifier

Yushuo Pei, Yu Tang, *Senior Member, IEEE*, Hucheng Xu, Jincai Niu, and Leijiao Ge, *Senior Member, IEEE*

***Abstract*—Carrier-based discontinuous pulsewidth modulation (PWM) is widely used in three-level ac/dc converters due to its features of higher efficiency and simpler implementation. However, the problems of switching losses, current distortion around zero-crossing points, and neutral-point (NP) voltage fluctuation are mutually coupled for the Vienna rectifier. Therefore, this article proposes a modified carrier-based discontinuous pulsewidth modulation (MCB-DPWM) scheme for the Vienna rectifier with improved zero-sequence voltage injection. The clamping range and clamping mode that suppress zero-crossing distortion are adjusted. Compared to continuous PWM and conventional discontinuous PWM, the proposed MCB-DPWM could effectively eliminate zero-crossing distortion and reduce the NP voltage fluctuation and switching loss, which means higher input current quality and efficiency. Moreover, it features a simpler implementation and less computational burden than space-vector-based PWM. Therefore, it is more suitable for high-frequency applications. Finally, the simulation and experimental results demonstrate that the proposed MCB-DPWM could reduce switching loss and current distortion with lower NP voltage fluctuation under different modulation indices.**

***Index Terms*—Carrier-based discontinuous pulsewidth modulation (CB-DPWM), neutral-point (NP) voltage fluctuation, switching loss reduction, Vienna rectifier, zero-crossing distortion.**

I. Introduction

THE Vienna rectifier, as shown in Fig. 1, which is similar to the T-type converter, features similar benefits of current waveform quality and higher efficiency. Due to its high power density, high reliability, and low-blocking voltage stress, the three-phase Vienna rectifier has been widely adopted in a variety of applications, such as electric vehicle charging systems, telecommunication power systems, wind energy applications, and aircraft systems [1], [2], [3], [4], [5].

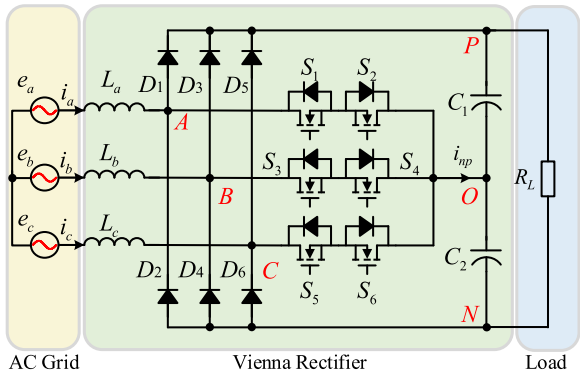

Fig. 1. Topology of the Vienna rectifier.

The high switching frequency can reduce the volume of passive devices and improve the power density of the converter, but it will increase the switching loss and affect the efficiency of the converter [6]. Compared to the traditional continuous pulsewidth modulation (CPWM), the discontinuous pulsewidth modulation (DPWM) makes the switches of each phase not operate within one-third of the fundamental cycle, reducing the switching loss. In addition, the high switching frequency leads to a shortened control period, which further increases the computational burden of the controller [7].

Fortunately, compared with the space-vector pulsewidth modulation (SV-PWM), carrier-based pulsewidth modulation (CB-PWM) can also achieve corresponding characteristics by injecting various zero-sequence components into the three-phase sinusoidal modulation signals without introducing the complexities of sector judgment, vector selection, and synthesis [8], [9]. Therefore, CB-PWM features a simpler implementation and less computational burden [10].

To achieve a higher efficiency, the DPWM can be adopted, which helps reduce the converter switching losses. In [11], a DPWM method using two different offsets was proposed for

Manuscript received 22 February 2023; revised 15 May 2023 and 25 June 2023; accepted 20 July 2023. Date of publication 25 July 2023; date of current version 1 September 2023. This work was supported in part by the Hebei Province Science Fund for Distinguished Young Scholars under Grant E2020202140, in part by the National Natural Science Foundation of China under Grant 51677084, and in part by the Hebei Provincial Central Government Guided Local Science and Technology Development Fund Project under Grant 216Z4401G. Recommended for acceptance by S. Mekhilef. *(Corresponding authors: Yu Tang; Leijiao Ge.)*

Yushuo Pei, Yu Tang, Hucheng Xu, and Jincai Niu are with the State Key Laboratory of Reliability and Intelligence of Electrical Equipment, Hebei University of Technology, Tianjin 300130, China, and also with the Hebei Key Laboratory of Electromagnetic Field and Electrical Apparatus Reliability, Hebei University of Technology, Tianjin 300401, China (e-mail: 202121401099@stu.hebut.edu.cn; zgsjit@163.com; 202131404080@stu.hebut.edu.cn; 202211401018@stu.hebut.edu.cn).

Leijiao Ge is with the Tianjin University, Tianjin 300350, China (e-mail: legendglj99@tju.edu.cn).

Color versions of one or more figures in this article are available at https://doi.org/10.1109/TPEL.2023.3298827.

Digital Object Identifier 10.1109/TPEL.2023.3298827

less switching losses in three-level neutral-point (NP) clamped inverters. Therefore, efficiency higher than the conventional CPWM approach was obtained due to the decreased number of switching operations. In [12], a simple DPWM for a three-level inverter was proposed, which can maintain low switching losses and perform effective voltage balancing without intricate calculations. In [13], an analytical DPWM-based simplified subsector identification was presented, which has high efficiency and comparatively low-current harmonics. However, the above strategies are not appropriate for the Vienna rectifier, whose force-commutated characteristic will lead to current distortion in zero-crossing areas [14]. A DPWM method for three-phase Vienna rectifiers was presented in [15] to maximize the switching loss reduction by keeping the phase with the highest phase current unswitched. However, the ability of this DPWM method to balance the NP voltage and reduce current distortion should be enhanced.

Due to its semicontrolled characteristic, the reference voltage and the input current near the zero-crossing point have opposite signs, resulting in additional current distortion [16], [17]. Clamping the leg generating pulses with a sign opposite to the NP is an effective approach to reducing zero-crossing current distortion [18], [19], [20], [21], [22], [23]. In [18], the implementation of a DPWM strategy explained by means of space-vector representation and modulation functions was presented. The zero-crossing distortion can be reduced by using this method, and a detailed comparison of the current waveform quality to CPWM was made. In order to decrease the computational burden, an equivalent carrier-based implementation of this method without sector judgment and the calculation of dwell time was proposed in [19]. However, the large zero-crossing clamp intervals in the low- and medium-modulation indices cause a dominant third harmonic in NP current, hence resulting in a poorer harmonic performance of the input current. In [20], a carrier-based discontinuous space-vector modulation (CB-DSVM) with varying clamped area was proposed, which can reduce the clamped area around zero crossing and get lower input current total harmonic distortion (THD). However, the setting of clamped areas under different modulation indices is not discussed in detail. In [21], a variable $d_{\mathrm{PF.X}}$ was introduced to detect the phase-X input current and voltage directions. As a result, when $d_{\mathrm{PF.X}} = 0$, the phase-X voltage was clamped to X-O to eliminate zero-crossing distortion. A hybrid modulation method, which consists of adding a special zero sequence to the reference signal during certain intervals, was presented in [22]. By using this method, the current distortion of the Vienna rectifier can be reduced without restricting the modulation index. Similarly, a zero-sequence component injection approach that can effectively lower input current distortion was suggested in [23]. However, the identification of abnormal intervals suffers from calculation complexity.

The quality of the input current is also influenced by the NP fluctuation. A larger third fluctuation of NP voltage introduces low-frequency current harmonics, resulting in higher input current THD. Compared with adding more electrolytic capacitors, software-based solutions are preferred to suppress the NP fluctuation, which can improve the power density. Both CB-PWM and SV-PWM schemes have been used to reduce NP oscillation, and their basic underlying ideas are similar in which they both adjust the switching sequence and dwell time of vectors to control the current flowing into the NP. A novel CB-PWM with segmented component injection was proposed in [24], which cannot only suppress the dc-link voltage oscillation but also maintain input current with minimal harmonic distortion. In [25], a hybrid NP balancing control scheme combining a dynamic adjustment factor was proposed. Through this method, the problem of NP fluctuation can be effectively solved in the Vienna rectifier. Unfortunately, the improvement in the efficiency of these methods has not been investigated. In [16], a hybrid discontinuous modulation strategy combining two DPWMs was proposed, which can reduce switching losses and midpoint potential fluctuations. However, this strategy is implemented based on the space-vector method, and the switching angles of the two DPWMs need to be calculated under different modulation indices, resulting in complicated implementation steps and a large amount of calculation.

In summary, the problems of current distortion around zero-crossing points, NP voltage fluctuation, and switching losses are mutually coupled for the Vienna rectifier. As a result, the carrier-based discontinuous modulation strategy for the Vienna rectifier with improved current quality and higher efficiency needs further research.

This article proposes a modified carrier-based DPWM (MCB-DPWM) strategy with reduced switching loss and current distortion. The proposed MCB-DPWM strategy with improved zero-sequence voltage injection will do the following:

1) reduce the switching losses of the power semiconductors by using the clamping modes with lower switching losses;
2) eliminate the input current zero-crossing distortion by clamping the zero-crossing phase in adjustable clamping regions;
3) suppress the NP low-frequency fluctuation by adjusting the clamping modes with opposite NP deviation in subsectors 1, 2, 3, and 4;
4) reduce the computational burden and implementation complexity as the carrier-based modulation is used.

The rest of this article is organized as follows. In Section II, the space-vector modulation method and carrier-based modulation of the Vienna rectifier are introduced and compared. In Section III, an MCB-DPWM strategy is proposed, and the performance of the proposed MCB-DPWM is analyzed in terms of switching loss reduction, zero-crossing distortion elimination, and NP fluctuation suppression. Moreover, the implementation of the MCB-DPWM is given in detail. In Section IV, simulation and experimental results are presented to validate the performance of the proposed modulation strategy. Finally, Section V concludes this article.

II. Modulation Methods of Vienna Rectifier

A. Space-Vector Modulation Method

The space-vector diagram of the Vienna rectifier is shown in Fig. 2. Each large sector I–VI in Fig. 2 can be divided into six subsectors. The terminal voltages u_{XO} ($X = A, B, C$) are

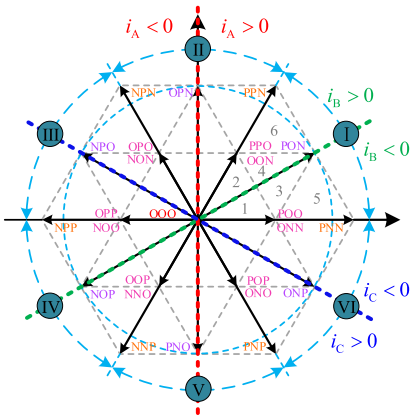

Fig. 2. Space-vector diagram of Vienna rectifier.

TABLE I
SWITCHING STATE AND TERMINAL VOLTAGE

Switching State	*Device Switching Status*	*Current Direction (x=a, b, c)*	*Terminal Voltage*
P	OFF	i_x>0	$U_{dc}/2$
O	ON	i_x>0	0
		i_x<0	
N	OFF	i_x<0	$-U_{dc}/2$

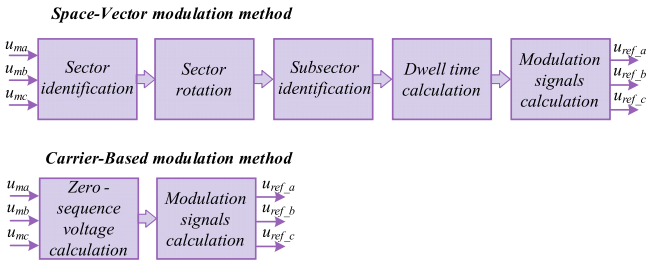

Fig. 3. Calculation process of SV-PWM and CB-PWM in digital control.

determined by the state of the bidirectional switching unit and current i_x, ($x = a, b, c$). Three switching states P, O, and N correspond to the terminal voltage $U_{dc}/2$, 0, $-U_{dc}/2$, respectively. Table I presents the relationship between the switching state and terminal voltage. The terminal voltage u_{XO} ($X = A, B, C$) is defined as follows:

$$u_{XO} = \text{sign}\,(i_x) \cdot (1 - S_x) \cdot U_{dc}/2, \quad x = a, b, c. \tag{1}$$

The reference voltage vector can be presented as follows:

$$\begin{aligned} V_{ref} &= 2/3 \cdot \left(u_{AO} + u_{BO}e^{j2\pi/3} + u_{CO}e^{j4\pi/3}\right) \\ &= |V_{ref}|\, e^{j\omega t}. \end{aligned} \tag{2}$$

B. Carrier-Based Modulation Method

The calculation processes of the space-vector-based and carrier-based modulation methods are shown in Fig. 3. For the space-vector-based modulation methods, apart from the sector identification and rotation similar to the conventional SVPWM, the identification conditions of subsectors are more complicated for advanced modulation methods. Additionally, a significant number of trigonometric function calculations are involved in the calculation of vector dwell time, resulting in a significant stress on the digital signal processor. However, the first four calculation processes of space-vector-based modulation methods can be equivalent to a zero-sequence voltage calculation process, and the zero-sequence voltage calculation of carrier-based modulation methods only requires simple calculations. Therefore, compared with the space-vector-based modulation methods, the computational complexity of the carrier-based modulation methods is simpler and less burdensome.

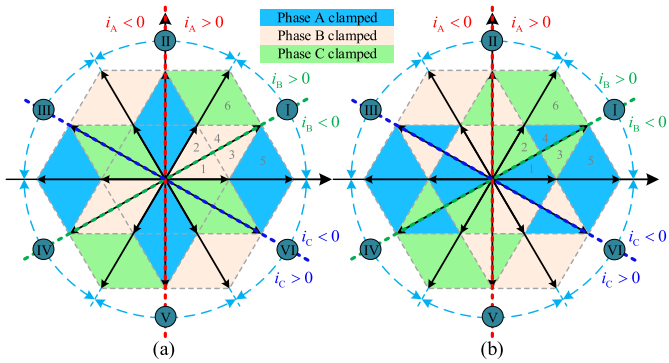

Fig. 4. Clamping modes of DPWM1 and DPWM2. (a) DPWM1. (b) DPWM2.

Carrier-based modulations can be achieved by injecting different zero-sequence voltages into the three-phase sinusoidal modulation wave. The normalized three-phase sinusoidal modulation signals are u_{ma}, u_{mb}, and u_{mc}, as shown in (3), where ω is the angular frequency of utility grid voltage. The modulation index m can be calculated by (4)

$$\begin{cases} u_{ma} = \frac{2}{\sqrt{3}} m \cos(\omega t) \\ u_{mb} = \frac{2}{\sqrt{3}} m \cos(\omega t - 2\pi/3) \\ u_{mc} = \frac{2}{\sqrt{3}} m \cos(\omega t - 4\pi/3) \end{cases} \tag{3}$$

$$m = \frac{\sqrt{3} U_m}{U_{dc}} \tag{4}$$

where U_m represents the amplitude of utility grid voltage, and U_{dc} represents the dc-link voltage.

Two commonly used DPWM methods for three-level Vienna rectifiers are DPWM1 and DPWM2 [15], [18], and Fig. 4 shows the clamping modes of these two methods. The carrier-based implementation method for the conventional DPWM1, where the zero-sequence voltage is given, can be calculated by [19]

$$u_z = \begin{cases} -u_{mid}, & |u_{max}| \geq |u_{min}|, u_{z1} > -u_{mid} \\ 1 - u_{max}, & |u_{max}| \geq |u_{min}|, u_{z1} < -u_{mid} \\ -u_{mid}, & |u_{max}| < |u_{min}|, u_{z1} < -u_{mid} \\ -1 - u_{min}, & |u_{max}| < |u_{min}|, u_{z1} > -u_{mid} \end{cases} \tag{5}$$

where $u_{\max}$, u_{mid}, and $u_{\min}$ represent the maximum, medium, and minimum values of u_{mx}, respectively, and u_{z1} can be represented as follows:

$$u_{z1} = \begin{cases} 1 - u_{\max}, & |u_{\max}| \geq |u_{\min}| \\ -1 - u_{\min}, & |u_{\max}| < |u_{\min}| \end{cases}. \tag{6}$$

The modulation wave of the conventional DPWM1 can be obtained by injecting (5) into (3), as shown in (7). u_{ref_x} $(x = a,b,c)$ is the modulation wave of CB-DPWM1

$$u_{\mathrm{ref}\_x} = u_{mx} + u_z, x = a, b, c. \tag{7}$$

This conventional CB-DPWM1 can keep the switches unswitched for some intervals to reduce switching losses. However, since CB-DPWM1 clamps the phase with the absolute value of the minimum current in subsectors 1, 2, 3, and 4, the reduction of switching losses is limited.

To further reduce switching losses, the best way is to clamp the phase with the absolute value of the maximum current. Consider sector 1 as an illustration, the relationship between the three-phase ac current in subsectors 1, 3, and 5 is $|i_a| > |i_c| > |i_b|$; therefore, phase-A should be clamped to reduce switching losses. Similarly, Phase-C should be clamped in subsectors 2, 4, and 6. However, in subsector 3, the three-phase currents $i_a > 0$, $i_b < 0$, and $i_c < 0$. The vector states are determined by the direction of the current, preventing the small vector PPO from being used and the phase-A from being clamped. Similarly, the small vector ONN cannot be used, and the phase-C cannot be clamped in subsector 4. Therefore, in subsectors 3 and 4, the best way to reduce switching losses for the Vienna rectifier is to clamp the phase with the absolute value of the medium current (phase-C in subsector 3 and phase-A in subsector 4).

The zero-sequence voltage of the CB-DPWM2 strategy can be calculated by

$$u_z = \begin{cases} 1 - u^*_{\max}, & u_{\mathrm{mid}} > 0, 1 + u_{\min} = u^*_{\mathrm{mid}} \\ -u^*_{\min}, & u_{\mathrm{mid}} > 0, \mathrm{else} \\ -u^*_{\min}, & u_{\mathrm{mid}} < 0, u_{\max} = u^*_{\mathrm{mid}} \\ 1 - u^*_{\max}, & u_{\mathrm{mid}} < 0, \mathrm{else} \end{cases} \tag{8}$$

where $u^*_{\max}, u^*_{\mathrm{mid}}$, and $u^*_{\min}$ represent the maximum, medium, and minimum values of u^*_{mx}, respectively, and u^*_{mx} can be represented as follows:

$$u^*_{mx} = \begin{cases} u_{mx}, & u_{mx} > 0 \\ u_{mx} + 1, & u_{mx} < 0 \end{cases} \quad x = a, b, c \quad . \tag{9}$$

However, due to the operation of the Vienna rectifier and the limitation of current sampling accuracy, the reference voltage of DPWM2 may be opposite to the input current near the zero-crossing point, resulting in zero-crossing current distortion [15], [22].

III. Modified Carrier-Based DPWM

A. Modified Carrier-Based DPWM

To eliminate the zero-crossing current distortion, suppress the NP fluctuation, and reduce the switching loss simultaneously, this article proposes an MCB-DPWM. The proposed MCB-DPWM divides the clamping areas into zero-crossing clamping areas and minimum switching loss areas. Various functions are achieved by injecting specific zero-sequence voltages in different areas.

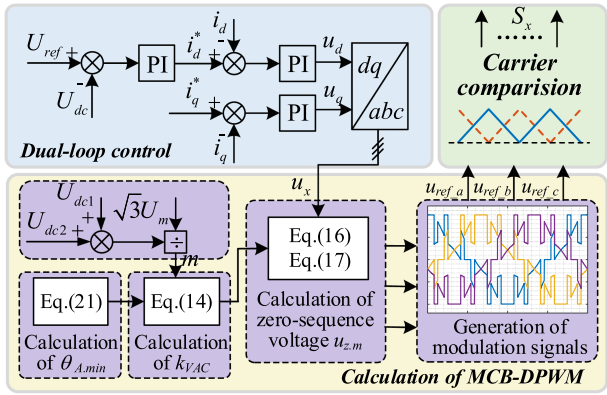

Fig. 5. Block diagram of the proposed MCB-DPWM scheme.

The block diagram of the proposed MCB-DPWM scheme is depicted in Fig. 5. U_{ref} and U_{dc} represent the reference output voltage and the feedback output voltage, respectively. i^*_d and i^*_q represent the d-axis and q-axis components of the reference input current, respectively. i_d and i_q represent the d-axis and q-axis components of the feedback input currents, respectively. u_d and u_q represent the output voltages of dual-loop control in dq coordinate system. u_x $(x = a, b, c)$ represents the sine modulation signals in abc-coordinate. U_{dc1} and U_{dc2} represent the voltages of the upper and lower capacitors, respectively. u_{ref_x} $(x = a, b, c)$ represents the modulation signals generated by MCB-DPWM. S_x represents the driving signals of the switching devices.

To reduce the zero-crossing current distortion, the phase reference voltages need to be clamped to 0 near the current zero-crossing point. In the zero-crossing clamping region, the injected zero-sequence voltage is defined as the zero-crossing clamping voltage u_{oc}, which can be calculated by

$$u_{oc} = -\mathrm{mid}\left\{u_{ma}, u_{mb}, u_{mc}\right\}. \tag{10}$$

To reduce switching losses, the phase with the maximum or medium absolute value of the current needs to be clamped. The zero-sequence voltage injected in the minimum switching loss areas can be calculated by (8).

As mentioned above, DPWM1 can eliminate the zero-crossing current distortion. However, a large zero-crossing clamping area of DPWM1 will lead to a significant NP fluctuation and poor current THD. Moreover, a large zero-crossing clamping area limits the reduction of switching losses. Therefore, it is crucial to control the size of the zero-crossing clamping area. In order to solve this problem, the zero-crossing clamping area needs to be kept within a range that can eliminate the zero-crossing current distortion without significantly raising switching losses or NP fluctuation. MCB-DPWM can use appropriate variable area clamping values to adjust the size of the zero-crossing clamping area.

The region of the zero-crossing clamping can be adjusted by adding u_{th} to the zero-sequence voltage injection condition,

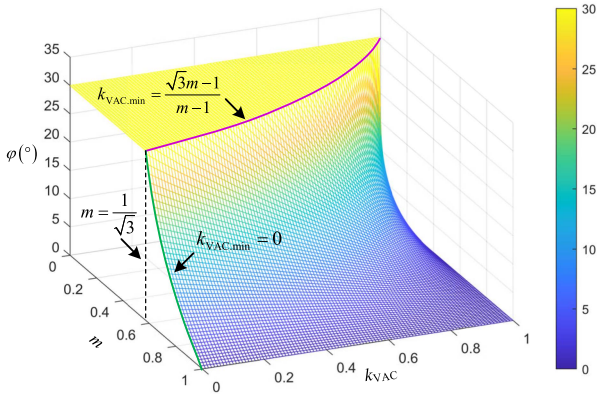

Fig. 6. Relationship among m, k_{VAC}, and φ.

which can be expressed as follows:

$$1-u_{\max}+u_{\mathrm{mid}}-u_{th}=0 \tag{11}$$

where $u_{\max}$ and u_{mid} represent the maximum and medium values of u_{mx}. u_{th} can be calculated by

$$u_{th}=k_{\mathrm{VAC}}(1-m) \tag{12}$$

where k_{VAC} is the variable area clamping coefficient.

Using sector 1 as an illustration, $\omega t=\pi/6-\varphi$, $u_{\max}$, and u_{mid} can be expressed as follows:

$$\begin{cases} u_{\max}=u_{ma}=\frac{2m\cos(\pi/6-\varphi)}{\sqrt{3}} \\ u_{\mathrm{mid}}=u_{mc}=\frac{2m\cos(-2\pi/3+\pi/6-\varphi)}{\sqrt{3}}. \end{cases} \tag{13}$$

After substituting (12) and (13) into (11), the variable area clamping coefficient k_{VAC} can be obtained by

$$k_{\mathrm{VAC}}=\frac{m\cos(\varphi)+\sqrt{3}m\sin(\varphi)-1}{m-1}. \tag{14}$$

The variable area clamping coefficient k_{VAC} should satisfy the condition $k_{\mathrm{VAC.min}}<k_{\mathrm{VAC}}<1$. When $k_{\mathrm{VAC}}\le k_{\mathrm{VAC.min}}$, the MCB-DPWM operates in the same clamping mode as the CB-DPWM1. $k_{\mathrm{VAC.min}}$ can be calculated by

$$k_{\mathrm{VAC.min}}=\begin{cases} \frac{\sqrt{3}m-1}{m-1}, & 0<m<\frac{1}{\sqrt{3}} \\ 0, & \frac{1}{\sqrt{3}}<m<1. \end{cases} \tag{15}$$

The relationship among m, k_{VAC}, and φ is seen in Fig. 6. Through altering the variable area clamping coefficient k_{VAC} under various modulation index m, the zero-crossing clamping angle could be changed.

The principle of utilizing u_{th} to adjust the clamping area is also demonstrated in Fig. 7. The adjustable range of the MCB-DPWM zero-crossing clamp area is depicted in blue in Fig. 7, and the width of the clamp area may be adjusted by modifying the value of u_{th}. The zero-crossing clamping area, which is purple shaded, is at its largest for $u_{th}=0$ ($k_{\mathrm{VAC}}=k_{\mathrm{VAC.min}}$), while there is no zero-crossing clamping area for $u_{th}=1-m$ ($k_{\mathrm{VAC}}=1$).

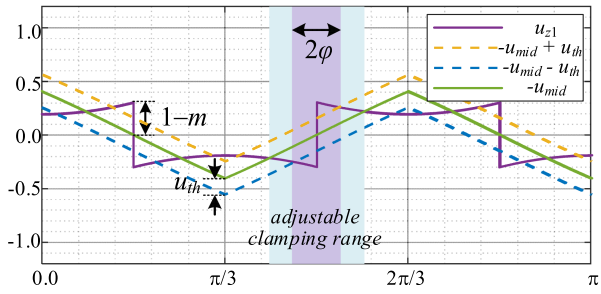

Fig. 7. Adjustable clamping range of MCB-DPWM.

TABLE II
MODULATION SIGNAL OF MCB-DPWM IN SECTOR I

Subsector	u_{ref_a}	u^*_{max}	u^*_{min}	u_{mid}
1*a*	$u_{ma}-u^*_{min}$	u^*_{mb}	u^*_{ma}	<0
1*b*	$u_{ma}-u_{mid}$	u^*_{mb}	u^*_{ma}	<0
2*a*	$u_{ma}-u^*_{max}+1$	u^*_{mc}	u^*_{mb}	>0
2*b*	$u_{ma}-u_{mid}$	u^*_{mc}	u^*_{mb}	>0
3*a*	$u_{ma}-u^*_{min}$	u^*_{mb}	u^*_{mc}	<0
3*b*	$u_{ma}-u_{mid}$	u^*_{mb}	u^*_{mc}	<0
4*a*	$u_{ma}-u^*_{max}+1$	u^*_{ma}	u^*_{mb}	>0
4*b*	$u_{ma}-u_{mid}$	u^*_{ma}	u^*_{mb}	>0
5	$u_{ma}-u^*_{max}+1$	u^*_{ma}	u^*_{mc}	<0
6	$u_{ma}-u^*_{min}$	u^*_{ma}	u^*_{mc}	>0

When $u_{\mathrm{mid}}<0$, the zero-sequence voltage of the MCB-DPWM is determined by

$$u_{z.m}=\begin{cases} -u_{\mathrm{mid}}, & u_{z1}>-u_{\mathrm{mid}}+u_{th} \\ 1-u^*_{\max}, & u_{z1}<-u_{\mathrm{mid}}+u_{th}, u_{\max}=u^*_{\max} \\ -u^*_{\min}, & u_{z1}<-u_{\mathrm{mid}}+u_{th}, \text{else}. \end{cases} \tag{16}$$

When $u_{\mathrm{mid}}>0$, the zero-sequence voltage of the MCB-DPWM is determined by

$$u_{z.m}=\begin{cases} -u_{\mathrm{mid}}, & u_{z1}<-u_{\mathrm{mid}}-u_{th} \\ -u^*_{\min}, & u_{z1}>-u_{\mathrm{mid}}-u_{th}, 1+u_{\min}=u^*_{\min} \\ 1-u^*_{\max}, & u_{z1}>-u_{\mathrm{mid}}-u_{th}, \text{else}. \end{cases} \tag{17}$$

where $u_{\max}$, u_{mid}, and $u_{\min}$ represent the maximum, medium, and minimum values of u_{mx}, respectively. $u^*_{\max}$, u^*_{mid}, and $u^*_{\min}$ represent the maximum, medium, and minimum values of u^*_{mx}, respectively, and u^*_{mx} can be calculated by (9).

Then, the three-phase sinusoidal modulation signals are injected with the zero-sequence voltage derived from (16) and (17) to produce the MCB-DPWM modulated signals

$$u_{\mathrm{ref}\_x}=u_{mx}+u_{z.m}, x=a,b,c. \tag{18}$$

Fig. 8 shows the zero-sequence voltage and modulation waveforms of MCB-DPWM with $m=0.4$, $k_{\mathrm{VAC}}=0.8$, and $m=0.7$, $k_{\mathrm{VAC}}=0.5$. The intermediate variable equivalence conditions and modulated signals generation of clamping intervals 1*a*, 1*b*, 2*a*, 2*b*, 3*a*, 3*b*, 4*a*, 4*b*, 5, and 6 in sector I are shown in Table II and Fig. 8. As shown in Fig. 8, the MCB-DPWM clamps consistently close to the peak and zero-crossing points, which helps minimize switching losses and get rid of zero-crossing current distortion.

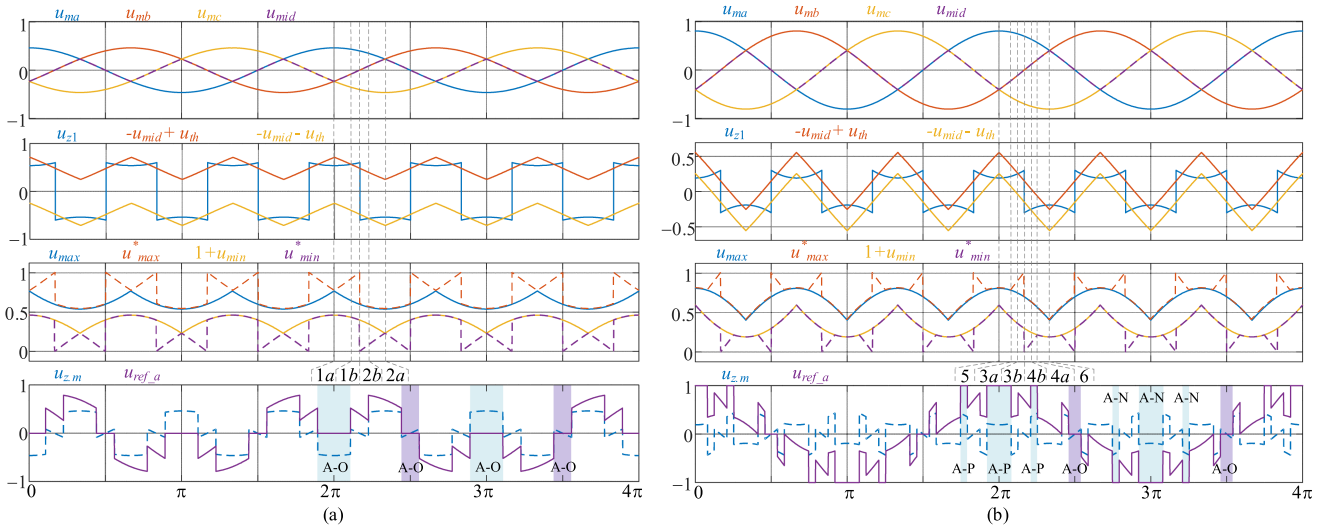

Fig. 8. Modulation waveforms of the MCB-DPWM under (a) $m = 0.4$ and $k_{\mathrm{VAC}} = 0.8$ and (b) $m = 0.7$ and $k_{\mathrm{VAC}} = 0.5$.

The NP voltage fluctuation suppression performance of the MCB-DPWM is described in Section III-D.

B. Zero-Crossing Distortion

The phase difference between the reference voltage and input current can be expressed as follows:

$$\theta_A = \theta_Z + \theta_{pf} \tag{19}$$

where θ_Z and θ_{pf} stand for the phase angle difference brought on by the impedance of the filter inductor and the nonunity power factor, respectively.

Due to the existence of the phase angle difference, the direction of the reference voltage and the input current may be opposite. Considering sector I, as an illustration, it is essential to clamp phase-B to O close to the current zero-crossing point of phase-B. Additionally, the clamping mode B-O needs to satisfy

$$\begin{cases} |\theta_A| \le \frac{\pi}{6}, & 0 < m < \frac{\sqrt{3}}{3} \\ |\theta_A| \le \arcsin\left(\frac{1}{2m}\right) - \frac{\pi}{6}, & \frac{\sqrt{3}}{3} \le m < 1. \end{cases} \tag{20}$$

Moreover, an excessively wide zero-crossing clamping angle will lead to poor input current quality as a result of the influence of the switching device snubber circuit and parasitic characteristics [20]. The existing zero-crossing current distortion can be avoided by increasing the MCB-DPWM zero-crossing clamping angle above the minimum zero-crossing clamping angle $\theta_{A,\min}$, which can be calculated by

$$\theta_{A.\min} = \theta_{pf.\min} + \theta_Z. \tag{21}$$

Thus, MCB-DPWM can keep the zero-crossing clamping angle within a small range, which can not only eliminate the zero-crossing current distortion but also reduce the NP potential fluctuation, hence improving the quality of the input current.

C. Switching Loss Comparison

For the accurate evaluation of switching losses for different modulation methods, the switching model and calculation method of switching loss in this article are the same as [21]. It has been proved that the calculated switching loss could be used to verify the efficiency of the Vienna rectifier by comparing the calculated switching energy with the switching energy data provided by the MOSFET manufacturer.

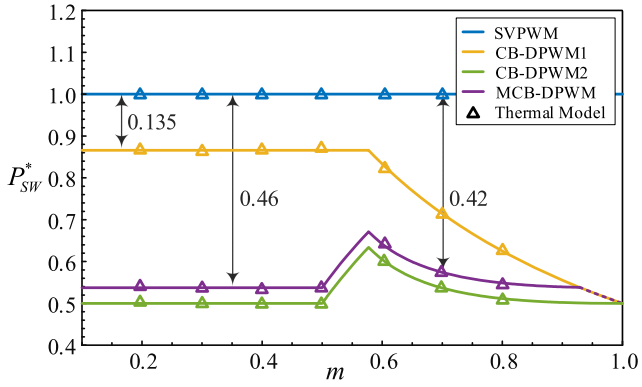

Fig. 9. Switching losses comparison of SVPWM, CB-DPWM1, CB-DPWM2, and MCB-DPWM.

To further verify the effectiveness of the calculated switching losses, a thermal model was built in PLECS using the thermal datasheets provided by the semiconductor manufacturer.

The switching loss of SVPWM is used as the benchmark, defined as $P_{\mathrm{loss,SW,SVPWM}}$, then the nominal switching losses of other modulation schemes can be expressed as follows:

$$P^*_{\mathrm{SW}} = P_{\mathrm{SW}} / P_{\mathrm{loss,SW,SVPWM}}. \tag{22}$$

The nominal results of the calculated and thermally simulated switching losses are shown in Fig. 9. As seen in Fig. 9, the evaluated switching losses agree well with the relative values of the calculation results. From Fig. 9, it can be seen that compared with the conventional SVPWM, the proposed MCB-DPWM scheme can effectively reduce the switching loss with different modulation indices at rated power. Due to the existence of the

adjustable zero-crossing clamping area, the switching loss of MCB-DPWM is slightly higher than that of CB-DPWM2. When CB-DPWM1 is adopted under $m < 0.5$, the phase with the minimum absolute value of current can be clamped, and the switching loss can only be decreased by 13.5%. After using the proposed MCB-DPWM, the switching loss can be reduced by 46% under $m < 0.5$ and 42% under $m = 0.7$. Except for the high-modulation indices, the switching loss of MCB-DPWM is also still lower than CB-DPWM1.

D. NP Voltage Fluctuation

Larger NP voltage low-frequency fluctuation for three-level converters may result in higher input current distortion and voltage stress on the devices [16]. Therefore, it is essential to maintain the NP voltage fluctuation at a lower level.

The NP voltage is determined by the current flowing into the midpoint of output capacitors, which can be expressed as follows:

$$i_{np} = \sum_{x=a,b,c} (i_x - u_{\text{ref\_}x} |i_x|) = - \sum_{x=a,b,c} u_{\text{ref\_}x} |i_x| \quad (23)$$

where $u_{\text{ref}\cdot x}$ $(x = a,b,c)$ is the modulation signal of different modulation methods. i_x, $(x = a, b, c)$ is the phase current.

The NP fluctuation can be calculated by

$$\Delta u_{\text{dc},nT_s} = u_{\text{dc1}} - u_{\text{dc2}} = -\frac{\int_{nT_s}^{(n+1)T_s} i_{np} dt}{2C}. \quad (24)$$

The nominal value of the NP fluctuation is presented as follows:

$$\Delta u^*_{\text{dc},nT_s} = \frac{\Delta u_{\text{dc},nT_s}}{I_{\text{peak}}/f_g 2C} \quad (25)$$

where f_g is the fundamental frequency, and C is the dc-link capacitor. I_{peak} is the peak value of the phase current.

The nominal NP fluctuation waveforms of CB-DPWM1, CB-DPWM2, and the proposed MCB-DPWM with various k_{VAC} under $m = 0.4$ and 0.7 are presented in Fig. 10. The nominal NP fluctuation waveforms of the MCB-DPWM, with $k_{\text{VAC}} \leq k_{\text{VAC.min}}$ (0.511 at $m = 0.4$, and 0 at $m = 0.7$), are same to that of the CB-DPWM1. Compared with the other DPWMs, the proposed MCB-DPWM with $k_{\text{VAC}} = 0.6$ has a lower NP oscillation at $m = 0.4$. The NP fluctuation peak value for the MCB-DPWM is equal to CB-DPWM2 and lower than CB-DPWM1 at $m = 0.7$. As a result, employing the MCB-DPWM will reduce the current low-frequency distortion caused by NP voltage fluctuation under various indices.

IV. Simulation and Experiments

A. Simulation Results

In order to verify the performance of the MCB-DPWM modulation method in eliminating the zero-crossing distortion of the ac current, suppressing NP fluctuation, and reducing switching losses, a 5-kW Vienna rectifier simulation model was built using PLECS. The simulation parameters are presented in Table III.

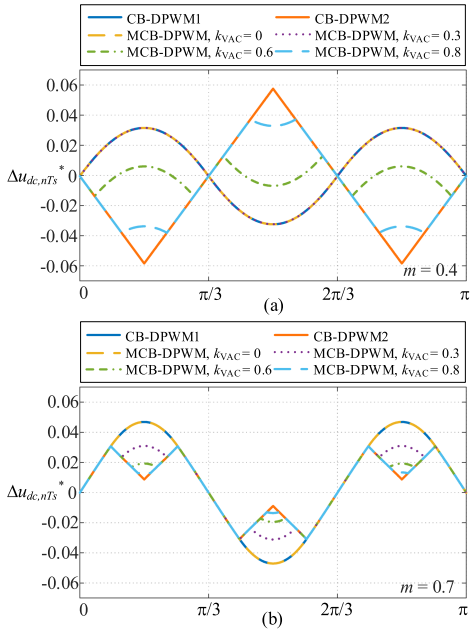

Fig. 10. Comparison of NP voltage fluctuation. (a) $m = 0.4$. (b) $m = 0.7$.

TABLE III
Parameters of the Vienna Rectifier

Parameter	*Value*
DC-link voltage	800 V
Rated input voltage	380 V ac
AC frequency	50 Hz
Switching frequency	30 kHz
Filter inductor	1.2 mH
DC-link capacitor	1000 μF

TABLE IV
Simulation Results of Different Modulation Schemes

Modulation	*Current THD* (%) $m = 0.4/m = 0.7$	*NP fluctuation* (V) $m = 0.4/m = 0.7$
SVPWM	2.26/1.94	±1.29/±1.35
CB-DPWM1	2.18/3.75	±12.08/±10.72
CB-DPWM2	4.66/3.12	±21.17/±6.17
MCB-DPWM	1.79/2.51	±11.86/±6.03

The simulation waveforms utilizing SVPWM, CB-DPWM1, CB-DPWM2, and MCB-DPWM with $m = 0.4$ and 0.7, respectively, are shown in Fig. 11. In these figures, i_a, i_b, and i_c represent the three-phase input currents. u_{AO} represents the voltage difference between terminals A and O in Fig. 1. u_{AB} represents the line voltage of phase AB. $u_{\text{ref}\cdot a}$ is the reference modulation signal of phase-A after injecting the zero-sequence voltage. Δu_{dc} represents the NP voltage fluctuation, which is the voltage difference between U_{dc1} and U_{dc2}. The corresponding simulation results for the current THD and NP voltage fluctuation are summarized in Table IV. The simulation waveforms of transient response under output power step-up and step-down conditions with different modulation methods are shown in Fig. 12. The transient response results show that the proposed

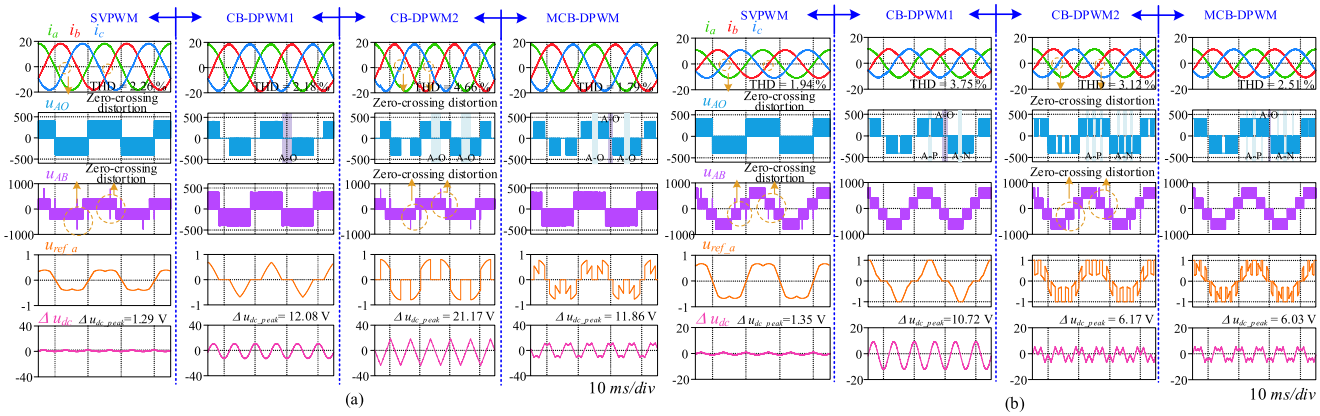

Fig. 11. Simulation waveforms of SVPWM, CB-DPWM1, CB-DPWM2, and MCB-DPWM. (a) $m = 0.4$. (b) $m = 0.7$.

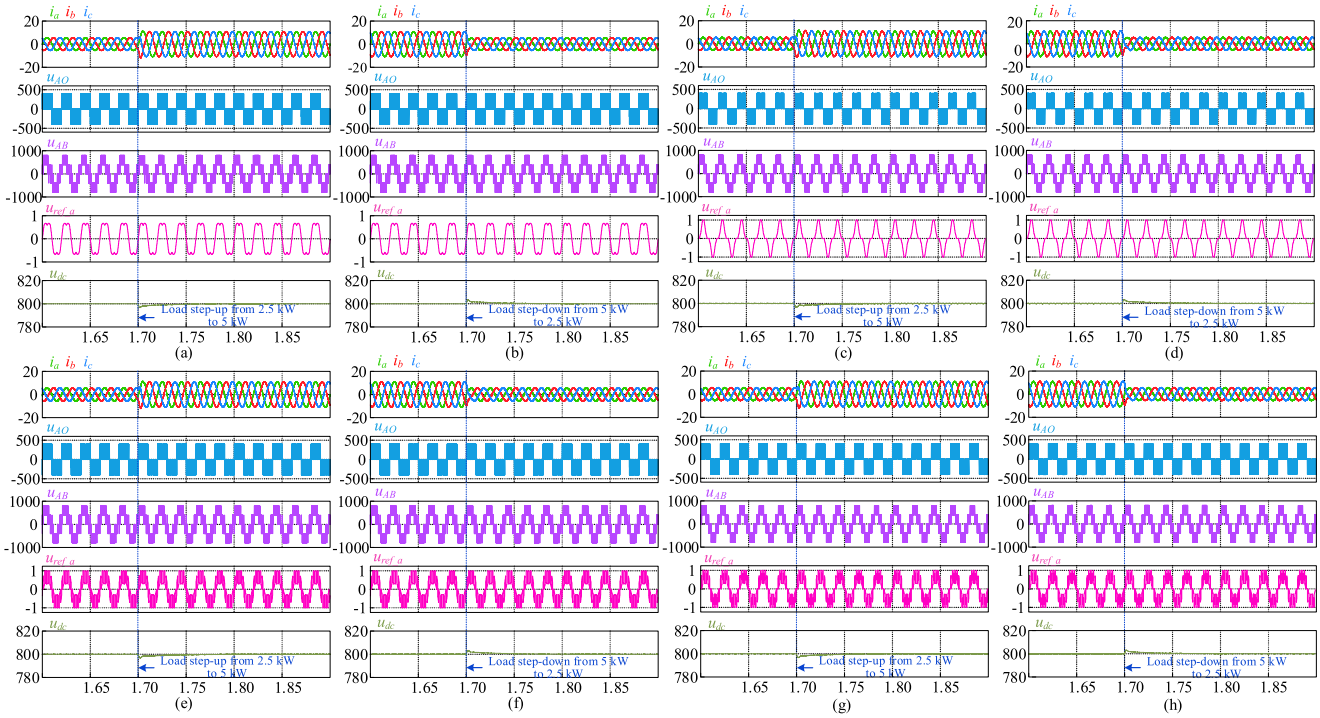

Fig. 12. Simulation waveforms of transient response under output power step-up and step-down conditions. (a) SVPWM with output power step-up from 2.5 to 5 kW. (b) SVPWM with output power step-down from 5 to 2.5 kW. (c) CB-DPWM1 with output power step-up from 2.5 to 5 kW. (d) CB-DPWM1 with output power step-down from 5 to 2.5 kW. (e) CB-DPWM2 with output power step-up from 2.5 to 5 kW. (f) CB-DPWM2 with output power step-down from 5 to 2.5 kW. (g) MCB-DPWM with output power step-up from 2.5 to 5 kW. (h) MCB-DPWM with output power step-down from 5 to 2.5 kW.

TABLE V
PARAMETERS OF THE EXPERIMENTAL PROTOTYPE

Part	*Device*
MOSFET (S_1 to S_6)	6 × OSG65R099HF
Diode (D_1 to D_6)	6 × C4D20120D
Gate driver	3 × UCC21520DW
Digital signal processor	1 × TMS320F280049C

TABLE VI
EXPERIMENTAL RESULTS OF DIFFERENT MODULATION SCHEMES

Modulation	*Current THD* (%) $m = 0.4/m = 0.7$	*NP fluctuation* (V) $m = 0.4/m = 0.7$
SVPWM	2.58/2.23	±1.39/±1.47
CB-DPWM1	2.42/4.08	±12.39/±11.12
CB-DPWM2	4.93/3.56	±21.03/±6.63
MCB-DPWM	2.05/2.63	±11.95/±6.55

MCB-DPWM has good dynamic response performance similar to other modulation methods.

Switching losses are effectively decreased in the purple clamping region close to the peak current point, thanks to the A-P, A-N, and A-O clamping modes. The modulated wave of SVPWM and CB-DPWM2 is not clamped near the current

TABLE VII
PROS AND CONS OF DIFFERENT MODULATION SCHEMES

Modulation	*Runtime/μs SV- /CB-*	*Zero-Crossing distortion*	*NP fluctuation* $m = 0.4/m = 0.7$	*Current THD* $m = 0.4/m = 0.7$	*Switching Loss*
SVPWM	4.05/2.07	Yes	Low/Low	Low/Low	High
DPWM1	4.12/2.34	No	Medium/High	Medium/High	Medium
DPWM2	4.28/2.09	Yes	High/Low	High/Medium	Low
MCB-DPWM	-----/2.16	No	Low/Low	Low/Low	Low

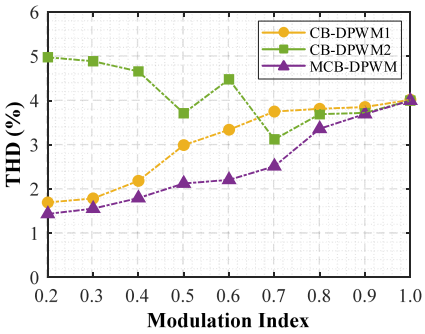

Fig. 13. Current THD of CB-DPWM1, CB-DPWM2, and MCB-DPWM in full-range modulation index.

zero-crossing point, as can be observed from the figures, which causes significant distortions in the three-phase input current and line voltage u_{AB}. Fortunately, since clamping mode A-O is employed in the blue-shaded region, the CB-DPWM1 and MCB-DPWM are able to completely eliminate the zero-crossing current distortion. NP voltage fluctuation for SVPWM, CB-DPWM1, CB-DPWM2, and MCB-DPWM is ±1.29 ±12.08, ±21.17, and ±11.86 V under $m = 0.4$, and ±1.35, ±10.72, ±6.17, and ±6.03 V under $m = 0.7$. In comparison with the other two discontinuous modulation methods, the MCB-DPWM has the lowest NP voltage fluctuation, which is nearly half of the maximum value among the three discontinuous modulation schemes. The MCB-DPWM has a lower NP voltage oscillation and no zero-crossing distortion, which reduces the low-frequency harmonics and results in the best current THD performance.

The current THD of CB-DPWM1, CB-DPWM2, and MCB-DPWM with different modulation indices is presented in Fig. 13. As can be seen from Fig. 13, the current THD is the same with $m = 1$, as the clamping modes are the same for the three DPWM methods with $m = 1$. However, the current THD of the proposed MCB-DPWM is lower than that of the other two DPWMs with both low- and medium-modulation indices. Especially in the range of modulation indices for practical applications ($0.4 < m < 0.8$), the current THD of MCB-DPWM is significantly lower than that of the other two discontinuous modulation methods. Therefore, MCB-DPWM has a lower current THD and better input current waveform quality than the other two discontinuous modulation methods.

Moreover, it is worth mentioning that using the proposed MCB-DPWM, the minimum switching loss, NP fluctuation reduction, and the zero-crossing distortion elimination are achieved simultaneously with different modulation indices.

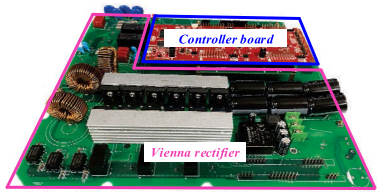

Fig. 14. Prototype of the three-phase Vienna rectifier.

B. Experimental Results

A 5-kW three-phase Vienna rectifier prototype, as shown in Fig. 14, was built to verify the theoretical analysis, and the main system parameters are the same as those of the simulation. The major devices used to build the hardware are listed in Table V.

The experimental results for different modulation schemes with modulation indices of 0.4 and 0.7 are shown in Fig. 15. The corresponding experimental results for the current THD and NP voltage fluctuation are summarized in Table VI. When SVPWM and CB-DPWM2 are used, the zero-crossing current distortion is visible at $m = 0.4$ and 0.7, as shown in Fig. 15(a), (c), (e), and (g). Comparing Fig. 15(b), (f), (d), and (g), both CB-DPWM1 and MCB-DPWM have no zero-crossing distortion. NP voltage fluctuation for SVPWM, CB-DPWM1, CB-DPWM2, and MCB-DPWM is ±1.39, ±12.39, ±21.03, and ±11.95 V under $m = 0.4$, and ±1.47, ±11.12, ±6.63, and ±6.55 V under $m = 0.7$. Therefore, there are smaller peaks of low-frequency neutral-point voltage fluctuations after using the proposed MCB-DPWM, which is nearly half of the maximum value among the three discontinuous modulation schemes. In all, the proposed MCB-DPWM has no zero-crossing distortion, smaller peaks of NP voltage fluctuation, and lower low-frequency harmonics, which results in a lower THD and better input current waveform quality.

The experimental waveforms of transient response under output power step-up and step-down conditions with different modulation methods are shown in Fig. 16. The dynamic response speed mainly depends on the control loop (dual-loop control used in this article), which has been proved in [26]. In fact, the control loop of four types of modulation methods is same, and the dynamic experimental effect of the proposed MCB-DPWM is almost the same as that of the other modulation methods.

The efficiency comparison among the SVPWM, the CB-DPWM1, the CB-DPWM2, and the proposed MCB-DPWM under $m = 0.7$ is depicted in Fig. 17. The peak efficiency of MCB-DPWM is 98.22%, and it is comparable with CB-DPWM2, which has a higher efficiency than the other modulation schemes.

The current THD comparison among the SVPWM, the CB-DPWM1, the CB-DPWM2, and the proposed MCB-DPWM

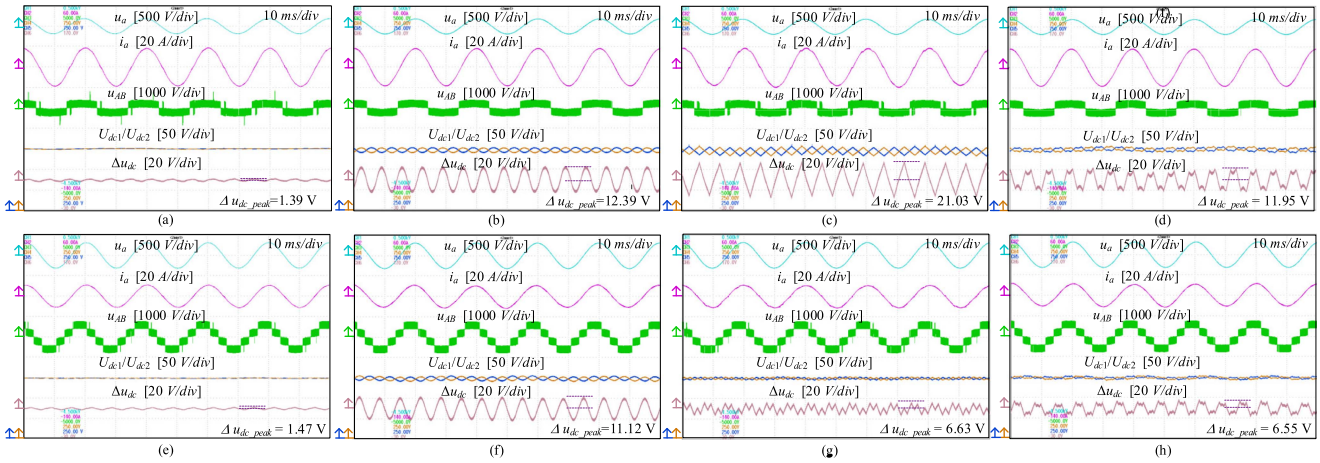

Fig. 15. Experimental results of SVPWM (a) and (e), CB-DPWM1 (b) and (f), CB-DPWM2 (c) and (g), MCB-DPWM (d) and (h) with (a)–(d) $m = 0.4$ and (e)–(h) $m = 0.7$.

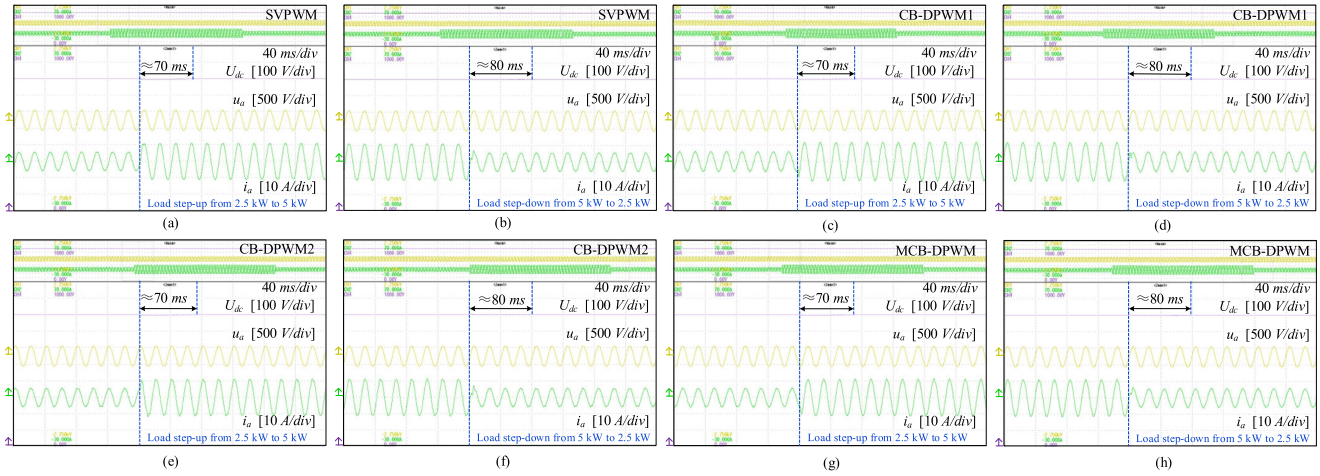

Fig. 16. Experimental waveforms of transient response under output power step-up and step-down conditions. (a) SVPWM with output power step-up from 2.5 to 5 kW. (b) SVPWM with output power step-down from 5 to 2.5 kW. (c) CB-DPWM1 with output power step-up from 2.5 to 5 kW. (d) CB-DPWM1 with output power step-down from 5 to 2.5 kW. (e) CB-DPWM2 with output power step-up from 2.5 to 5 kW. (f) CB-DPWM2 with output power step-down from 5 to 2.5 kW. (g) MCB-DPWM with output power step-up from 2.5 to 5 kW. (h) MCB-DPWM with output power step-down from 5 to 2.5 kW.

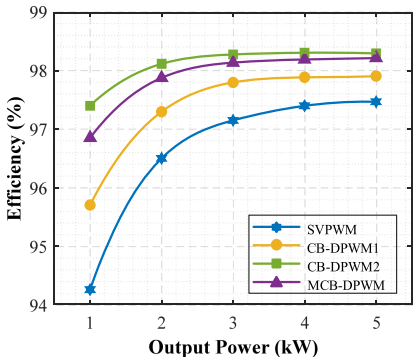

Fig. 17. Measured efficiencies of different modulation methods.

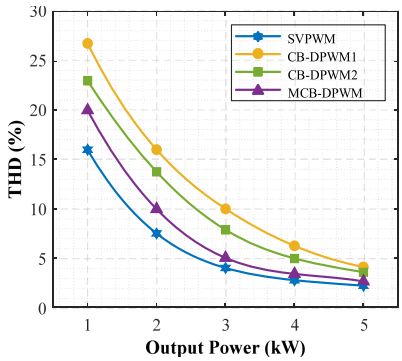

Fig. 18. Measured THDs of different modulation methods.

under $m = 0.7$ is depicted in Fig. 18. The MCB-DPWM has the lowest current THD among the three discontinuous modulation methods. At rated power, the current THD of the MCB-DPWM is slightly higher than that of the SVPWM and meets the standard of lower than 5%.

The pros and cons of different modulation methods are summarized in Table VII. The comparisons include program runtime based on the space-vector and carrier methods, whether there is zero-crossing distortion, NP fluctuation, and current THD with $m = 0.4$ and $m = 0.7$, and switching loss. SV- and CB- represent the space-vector-based and carrier-based implementations, respectively. The runtime of the conventional SVPWM is 4.05 μs, while the proposed MCB-DPWM takes only 2.16 μs. There is an almost 50% runtime reduction.

V. Conclusion

In this article, an MCB-DPWM is proposed for the Vienna rectifier by using the calculation of the proper zero-sequence components and division of the clamping area. Therefore, switching loss and current distortion are reduced simultaneously. Theoretical analysis and experimental results demonstrate the following characteristics of the proposed MCB-DPWM strategy.

1) The zero-crossing distortion can be eliminated by injecting the proper zero-sequence components in the adjustable clamping region, and the current THD performance is also improved.
2) The low-frequency NP voltage fluctuation is reduced after using the proposed MCB-DPWM. Therefore, the low-order harmonics of the input current are decreased, resulting in higher input current quality.
3) Compared with the conventional SVPWM, about 46% and 42% of switching losses are reduced with $m = 0.4$ and 0.7 by using the proposed MCB-DPWM.
4) Low computational burden and easy implementation, which is more accessible in practical applications.

The proposed MCB-DPWM performs well under normal utility grid condition, the optimizations of operational performance under unbalanced utility grid voltage conditions, and unbalanced load conditions are for further study. Moreover, as a requirement for high-frequency applications, simpler and more flexible carrier-based DPWM schemes are worthy of further research.

References

[1] J. W. Kolar and F. C. Zach, "A novel three-phase utility interface minimizing line current harmonics of high-power telecommunications rectifier modules," *IEEE Trans. Ind. Electron.*, vol. 44, no. 4, pp. 456–467, Aug. 1997.

[2] J. W. Kolar and T. Friedli, "The essence of three-phase PFC rectifier systems—Part I," *IEEE Trans. Power Electron.*, vol. 28, no. 1, pp. 176–198, Jan. 2013.

[3] A. Rajaei, M. Mohamadian, and A. Y. Varjani, "Vienna-rectifier-based direct torque control of PMSG for wind energy application," *IEEE Trans. Ind. Electron.*, vol. 60, no. 7, pp. 2919–2929, Jul. 2013.

[4] X. Xing, X. Li, C. Qin, Z. Liu, and C. Zhang, "Two-layer pulsewidth modulation strategy for common-mode voltage and current harmonic distortion reduction in Vienna rectifier," *IEEE Trans. Ind. Electron.*, vol. 67, no. 9, pp. 7470–7483, Sep. 2020.

[5] S. Xu, Z. Sun, C. Yao, H. Zhang, W. Hua, and G. Ma, "Model predictive control with constant switching frequency for three-level T-type inverter-fed PMSM drives," *IEEE Trans. Ind. Electron.*, vol. 69, no. 9, pp. 8839–8850, Sep. 2022.

[6] J. Wei, H. Xu, B. Zhou, Z. Zhang, and C. Gerada, "An integrated method for three-phase AC excitation and high-frequency voltage signal injection for sensorless starting of aircraft starter/generator," *IEEE Trans. Ind. Electron.*, vol. 66, no. 7, pp. 5611–5622, Jul. 2019.

[7] L. Hang, B. Li, M. Zhang, Y. Wang, and L. M. Tolbert, "Equivalence of SVM and carrier-based PWM in three-phase/wire/level Vienna rectifier and capability of unbalanced-load control," *IEEE Trans. Ind. Electron.*, vol. 61, no. 1, pp. 20–28, Jan. 2014.

[8] J. Pou, J. Zaragoza, S. Ceballos, M. Saeedifard, and D. Boroyevich, "A carrier-based PWM strategy with zero-sequence voltage injection for a three-level neutral-point-clamped converter," *IEEE Trans. Power Electron.*, vol. 27, no. 2, pp. 642–651, Feb. 2012.

[9] J. Pou, R. Pindado, D. Boroyevich, and P. Rodriguez, "Evaluation of the low-frequency neutral-point voltage oscillations in the three-level inverter," *IEEE Trans. Ind. Electron.*, vol. 52, no. 6, pp. 1582–1588, Dec. 2005.

[10] Y. Zou, L. Zhang, Y. Xing, Z. Zhang, H. Zhao, and Z. Zheng, "A unified carrier-based pulsewidth modulation for three-phase Vienna-type rectifiers," *IEEE Trans. Power Electron.*, vol. 37, no. 5, pp. 5749–5762, May 2022.

[11] J.-S. Lee, S. Yoo, and K.-B. Lee, "Novel discontinuous PWM method of a three-level inverter for neutral-point voltage ripple reduction," *IEEE Trans. Ind. Electron.*, vol. 63, no. 6, pp. 3344–3354, Jun. 2016.

[12] U.-M. Choi, H.-H. Lee, and K.-B. Lee, "Simple neutral-point voltage control for three-level inverters using a discontinuous pulse width modulation," *IEEE Trans. Energy Convers.*, vol. 28, no. 2, pp. 434–443, Jun. 2013.

[13] Q. Yan, L. Xiao, H. Chen, X. Yuan, H. Xu, and R. Zhao, "An analytical discontinuous space-vector PWM for three-level inverters with unbalanced DC-link voltages," *IEEE Trans. Power Electron.*, vol. 37, no. 7, pp. 7718–7728, Jul. 2022.

[14] Z. Zhang, O. C. Thomsen, and M. A. E. Andersen, "Discontinuous PWM modulation strategy with circuit-level decoupling concept of three-level neutral-point-clamped (NPC) inverter," *IEEE Trans. Ind. Electron.*, vol. 60, no. 5, pp. 1897–1906, May 2013.

[15] X. Zhang, Q. Wang, R. Burgos, and D. Boroyevich, "Discontinuous pulse width modulation methods with neutral point voltage balancing for three phase Vienna rectifiers," in *Proc. IEEE Energy Convers. Congr. Expo.*, 2015 pp. 225–232.

[16] Z. He et al., "A hybrid DPWM for Vienna rectifiers based on the three-level to two-level conversion," *IEEE Trans. Ind. Electron.*, vol. 69, no. 9, pp. 9429–9439, Sep. 2022.

[17] Q. Wang, X. Zhang, R. Burgos, D. Boroyevich, A. M. White, and M. Kheraluwala, "Design and implementation of a two-channel interleaved Vienna-type rectifier with >99% efficiency," *IEEE Trans. Power Electron.*, vol. 33, no. 1, pp. 226–239, Jan. 2018.

[18] L. Dalessandro, S. D. Round, U. Drofenik, and J. W. Kolar, "Discontinuous space-vector modulation for three-level PWM rectifiers," *IEEE Trans. Power Electron.*, vol. 23, no. 2, pp. 530–542, Mar. 2008.

[19] J.-S. Lee and K.-B. Lee, "Carrier-based discontinuous PWM method for Vienna rectifiers," *IEEE Trans. Power Electron.*, vol. 30, no. 6, pp. 2896–2900, Jun. 2015.

[20] W. Zhu, C. Chen, S. Duan, T. Wang, and P. Liu, "A carrier-based discontinuous PWM method with varying clamped area for Vienna rectifier," *IEEE Trans. Ind. Electron.*, vol. 66, no. 9, pp. 7177–7188, Sep. 2019.

[21] L. Zhang et al., "A modified DPWM with neutral point voltage balance capability for three-phase Vienna rectifiers," *IEEE Trans. Power Electron.*, vol. 36, no. 1, pp. 263–273, Jan. 2021.

[22] D. Molligoda et al., "Hybrid modulation strategy for the Vienna rectifier," *IEEE Trans. Power Electron.*, vol. 37, no. 2, pp. 1283–1295, Feb. 2022.

[23] W. Ding, C. Zhang, F. Gao, B. Duan, and H. Qiu, "A zero-sequence component injection modulation method with compensation for current harmonic mitigation of a Vienna rectifier," *IEEE Trans. Power Electron.*, vol. 34, no. 1, pp. 801–814, Jan. 2019.

[24] W. Ding, H. Qiu, B. Duan, X. Xing, N. Cui, and C. Zhang, "A novel segmented component injection scheme to minimize the oscillation of DC-link voltage under balanced and unbalanced conditions for Vienna rectifier," *IEEE Trans. Power Electron.*, vol. 34, no. 10, pp. 9536–9551, Oct. 2019.

[25] W.-Z. Song et al., "A hybrid control method to suppress the three-time fundamental frequency neutral-point voltage fluctuation in a Vienna rectifier," *IEEE J. Emerg. Sel. Topics Power Electron.*, vol. 4, no. 2, pp. 468–480, Jun. 2016.

[26] Q. Zhang, F. Liu, W. Jiang, J. Wang, and Y. Yue, "A novel modulation method based on model prediction control with significantly reduced switching loss and current zero-crossing distortion for Vienna rectifier," *IEEE Trans. Power Electron.*, vol. 38, no. 2, pp. 1650–1661, Feb. 2023.

Yushuo Pei was born in Shandong, China, in 1998. He received the B.S. degree from the School of Electrical Engineering, University of Jinan, Jinan, China, in 2021. He is currently working toward the M.S. degree in power electronics with the Hebei University of Technology, Tianjin, China.

His current research interests include the control and modulation of multilevel converters.

Yu Tang (Senior Member, IEEE) received the B.S. and Ph.D. degrees from the Department of Electrical Engineering, Nanjing University of Aeronautics and Astronautics (NUAA), Nanjing, China, in 2003 and 2008, respectively.

Since 2008, he has been with Electrical Engineering Department, NUAA, and the State Key Laboratory of State Key Laboratory of Reliability and Intelligence of Electrical Equipment, Hebei University of Technology, Tianjin, China, since 2018. He has authored or coauthored more than 80 papers in journals and conference proceedings. The research area includes power electronics in renewable energy generation.

Dr. Tang is the Guest Associate Editor for IEEE TRANSACTIONS ON POWER ELECTRONICS.

Hucheng Xu was born in Shandong, China, in 1998. He received the B.S. degree from the School of Electrical Engineering and Automation, Harbin University of Science and Technology, Weihai, China, in 2020. He is currently working toward the B.S. degree in power electronics with the Hebei University of Technology, Tianjin, China.

His current research interests include the control and modeling of dc–dc converters.

Jincai Niu received the M.S. degree from the School of Electrical and Information Engineering, Inner Mongolia University, Hohhot, China, in 2014. He is currently working toward the Ph.D. degree in power electronics with the Hebei University of Technology, Tianjin, China.

He is currently a Lecturer with the School of Electronic Engineering, Chaohu University, Hefei, China. His current research interests include power electronics technology and new energy generation technologies.

Leijiao Ge (Senior Member, IEEE) received the Ph.D. degree in electrical engineering from Tianjin University, Tianjin, China, in 2016.

He is currently an Associate Professor with the School of Electrical and Information Engineering, Tianjin University. His main research interests include smart distribution network, cloud computing, and Big Data.